Available online at www.sciencedirect.com
ScienceDirect
Earth and Planetary Science Letters 256 (2007) 162–168
EPSL
www.elsevier.com/locate/epsl

Thermoelastic properties of post-perovskite phase $MgSiO_3$ determined experimentally at core–mantle boundary P–T conditions

Nicolas Guignot [a,*], Denis Andrault [b], Guillaume Morard [a], Nathalie Bolfan-Casanova [c], Mohamed Mezouar [a]

[a] *ESRF, 6 Jules Horowitz, BP 220, 38043 Grenoble Cedex, France*
[b] *IMPMC, 140 rue de Lourmel, 75015 Paris, France*
[c] *Laboratoire Magmas et Volcans, 5 rue Kessler, 63038 Clermont-Ferrand Cedex, France*

Received 10 October 2006; received in revised form 21 December 2006; accepted 7 January 2007
Available online 27 January 2007
Editor: G.D. Price

Abstract

We have performed in-situ X-ray diffraction measurements on $MgSiO_3$ up to 144.5 GPa and 2535 K to obtain a precise experimental determination of the elastic properties of the post-perovskite polymorph of $MgSiO_3$ at high pressure and temperature. The complete dataset is comprised of 24 data points at ambient temperature and an equal number at high temperature. Fitted physical properties are the room temperature bulk modulus, the Grüneisen parameter with its volume dependency, the thermal expansion with its temperature dependency, and the linear incompressibilities as well as thermal expansions and their temperature dependency on each axis. Elastic anisotropy is observed, the structure being much more compressible along the *b* axis, and less compressible along the c axis, in agreement with theoretical calculations. We also demonstrate with the present study that experiments can provide precise information on the elasticity of complex materials at extreme pressure and temperature conditions.

Keywords: post-perovskite; equation of state; core–mantle boundary

1. Introduction

The recent discovery of a new $MgSiO_3$ high pressure polymorph [1,2] has had a considerable impact on our understanding of the structure and dynamics of the deep Earth's mantle. This post-perovskite phase with the *Cmcm* $CaIrO_3$ type-structure (hereafter noted ppv) is produced via phase transition from *Pbnm* perovskite $MgSiO_3$ at a pressure of 110–125 GPa. This corresponds roughly to the depth of the D″ layer, a mantle region where a very complex seismic signature has been reported, related mainly to a high lateral heterogeneity and shear-wave splitting (see [3] and references therein). The focus of our research is now to determine how much the occurrence of the ppv phase can explain these seismic anomalies, and which features remain to be explained by other possible sources like downwelling of the subducted slabs, partial melting of the mantle, or core–mantle chemical interactions. A major drawback is that the pressure and temperature conditions prevailing at those depths, about 135 GPa and possibly up to around 4000 K, are extremely high for accurate measurements of material properties. Ab-initio calculations have proved to be very

* Corresponding author. Tel.: +33 1 69 35 9747; fax: +33 1 69 35 9456.
E-mail address: guignot@synchrotron-soleil.fr (N. Guignot).

0012-821X/$ - see front matter © 2007 Elsevier B.V. All rights reserved.
doi:10.1016/j.epsl.2007.01.025

useful in obtaining this kind of information beyond the limit of experimental possibilities. They, however, often remain contradictory from one study to another. Here we present the first *P–V–T* equation of state of ppv performed at megabar pressures. The results are used to discuss the anisotropy properties of the ppv phase.

2. Experimental

The new ID27 beamline facilities at the ESRF (Grenoble) were used to collect in-situ high temperature angle-dispersive X-ray diffraction patterns of ppv at high pressure. A laser-heated diamond anvil cell, equipped with 100–300 μm beveled diamond anvils, combined with our new laser-heating setup (an evolution of the previous ID30 setup) [4,5], permitted data acquisition from 111 to 144.5 GPa with temperatures reaching 2535 K. The setup is composed of two 40 W single-mode continuous YAG lasers with excellent power stability focused on each side of the sample. This configuration is the best to minimize the axial, radial, and temporal temperature gradients within the sample. The X-ray beam intensity is sufficient to obtain high quality angle-dispersive diffraction patterns in less than 100 s, which further minimize any potential temperature deviation to a few tens of K. Note that a critical point with in-situ X-ray diffraction is the alignment of the laser hotspot with the focused X-ray beam (4×8 μm^2 spot, $\lambda=0.3738$ Å) during exposure. Due to radial temperature gradients, a misalignment of even a few microns can produce temperature measurement errors up to several hundreds of K. A perfect alignment is generally a problem because of the difficulty in imaging the monochromatic X-ray beam. This is however possible on ID27 because the very high flux excites the fluorescence of the diamond which enables visualization of the X-ray spot in the visible and UV range, thus allowing the X-ray/laser alignment with a precision at the micron level. The X-ray beam being very small and focused on the flat part of the Gaussian profile of the hot spot, the radial temperature gradient is considered to be negligible. We measured temperature on one side of the sample by the spectroradiometric method using reflective collecting optics. The methodology used and the accuracy of such temperature measurements are described by Benedetti and Loubeyre [6]. Errors given in Table 1 correspond to the standard deviation of the histogram of the two-color temperature [6] and the temperature deviation with time.

Mg_2SiO_4 powder has been used as starting sample and mixed with platinum for optimum laser absorption. We loaded that mixture in a 30 μm hole drilled in a Re gasket together with thin NaCl plates that serve as both pressure transmitting media and thermal isolators. Non-hydrostatic component of the applied pressure can be quantified by *St* values (multiplication of the elastic anisotropy factor *S* and the uniaxial stress term *t*) [7]. Values below 0.005 are usually considered to be poorly affected by non-hydrostaticity. Laser annealing performed during 10 min after each pressure increase kept deviatoric stresses minimal, with *St* value of 0.004 at 140.4 GPa and 2500 K (corresponding to the diffraction pattern displayed in Fig. 1) and 0.001 at 128.6 GPa and 300 K.

The detector used in this study is a MAR 345. The 2D diffraction images were integrated using Fit2D. The GSAS software [8] was used to refine the phases' unit-cell volumes.

3. Pressure measurement and formalisms

The free-MgO produced by the decomposition of Mg_2SiO_4 has been used to measure the pressure at any temperatures through the use of the *P–V–T* equation of state (EoS) of periclase. The classical way to describe the pressure at any given volume and temperature for a given phase is to decompose it into a room temperature term and a thermal pressure term. The MgO room temperature term used in this paper is a primary pressure scale [9,10]. Our initial choice of the MgO thermal pressure model based on several experiments done by Speziale et al. (2001) [10] yielded ppv thermal expansion values significantly higher than the ones obtained from ab-initio calculations. We can wonder however if this is real or linked to experimental uncertainties. An overestimation of MgO thermal expansion compared to different calculations [11,12] is for example visible in Fig. 12 of the paper. On the other hand, the thermal expansion values derived from these theoretical calculations as well as the one from another study [13] are compatible with each other, and almost undistinguishable in the megabar pressure range, though being generated from different calculation methods. Since all theoretical models are consistent, we chose the one from Karki et al. [12] to get thermal pressure of MgO at high temperature, and discarded Speziale et al. high temperature EoS. Note that the problem of pressure calibration is recurrent in the mineral physics community (see for example [27]). In the present case, the use of Speziale et al. model to extract the pressure at high temperature would yield pressures a few GPa higher than those obtained from our method. The pressure shift from actual pressures due to the choice of the pressure gauge is however unknown and we will only take into account the experimental error that comes from uncertainties in the

Table 1
P–V–T data on $MgSiO_3$ post-perovskite phase

P (GPa)	*a* (Å)	*b* (Å)	*c* (Å)	*V* (Å^3)	*T* (K)	a_{MgO} (Å)
111.1(5)	2.473584	8.105783	6.134658	123.00(8)	300	3.7522
114.8(5)	2.467492	8.089385	6.127964	122.32(7)	300	3.7437
115.4(5)	2.468392	8.080647	6.124279	122.16(7)	300	3.7423
117.4(5)	2.466453	8.071189	6.118184	121.80(10)	300	3.7380
118.5(5)	2.466175	8.060682	6.116515	121.59(5)	300	3.7355
118.2(5)	2.465687	8.063539	6.114923	121.58(5)	300	3.7361
117.9(5)	2.467123	8.065793	6.116477	121.71(6)	300	3.7368
121.7(5)	2.462973	8.047212	6.107080	121.04(3)	300	3.7285
123.0(5)	2.460243	8.042772	6.102291	120.75(4)	300	3.7258
123.3(5)	2.460619	8.039013	6.103719	120.74(8)	300	3.7252
123.5(5)	2.461332	8.037754	6.100445	120.69(8)	300	3.7248
123.8(5)	2.460076	8.039284	6.101700	120.67(4)	300	3.7240
124.0(5)	2.460758	8.035878	6.099467	120.61(4)	300	3.7236
127.5(5)	2.455981	8.018187	6.091888	119.96(3)	300	3.7163
129.5(5)	2.454011	8.009941	6.086818	119.65(4)	300	3.7122
129.5(5)	2.452957	8.010430	6.089190	119.65(3)	300	3.7122
128.6(5)	2.455264	8.018196	6.093702	119.97(5)	300	3.7140
129.1(5)	2.456719	8.004843	6.090545	119.77(4)	300	3.7129
129.4(5)	2.454427	8.010681	6.092878	119.80(4)	300	3.7123
131.4(5)	2.453198	7.994507	6.084594	119.33(4)	300	3.7082
131.6(5)	2.450566	7.996241	6.089450	119.32(5)	300	3.7079
132.0(5)	2.449594	7.995782	6.086390	119.21(5)	300	3.7070
132.4(5)	2.447289	8.004339	6.083857	119.18(4)	300	3.7063
132.4(5)	2.449522	7.993332	6.083714	119.12(4)	300	3.7063
121.2(1.3)	2.467457	8.092840	6.128891	122.39(5)	1435(100)	3.7448
121.4(1.0)	2.469872	8.089529	6.128890	122.46(8)	1556(60)	3.7462
124.5(1.3)	2.467560	8.071865	6.120382	121.90(6)	1511(100)	3.7387
130.0(1.3)	2.461717	8.044656	6.106192	120.92(4)	1569(100)	3.7275
135.8(1.1)	2.454950	8.013754	6.090868	119.83(5)	1468(60)	3.7139
134.7(1.0)	2.454899	8.019738	6.095531	120.01(5)	1508(60)	3.7167
137.5(0.9)	2.452777	8.000587	6.093049	119.57(4)	1496(50)	3.7107
122.5(1.0)	2.470041	8.086730	6.134717	122.54(4)	1663(50)	3.7456
124.0(1.1)	2.469941	8.091329	6.129780	122.50(7)	1872(70)	3.7455
125.2(1.2)	2.468495	8.081565	6.125894	122.21(8)	1857(80)	3.7426
125.9(1.3)	2.470325	8.082417	6.123755	122.27(7)	2015(90)	3.7435
127.8(1.4)	2.463649	8.087713	6.124510	122.03(3)	2040(100)	3.7396
134.0(1.7)	2.461169	8.046782	6.106779	120.94(3)	2059(140)	3.7265
134.3(1.3)	2.460057	8.042340	6.103836	120.76(4)	1973(90)	3.7244
139.1(1.2)	2.454031	8.018744	6.093710	119.91(4)	1984(80)	3.7146
141.1(1.1)	2.453369	7.999222	6.089490	119.51(4)	2023(60)	3.7111
134.0(1.8)	2.461477	8.047301	6.107495	120.98(5)	2134(150)	3.7275
137.2(0.9)	2.455503	8.026113	6.099758	120.21(5)	2082(50)	3.7199
143.7(1.2)	2.453575	7.999313	6.093167	119.59(4)	2438(80)	3.7119
128.7(1.3)	2.469960	8.090684	6.131126	122.52(5)	2455(100)	3.7442
130.2(1.7)	2.469278	8.083961	6.127606	122.32(3)	2511(140)	3.7418
137.3(1.8)	2.461784	8.047246	6.106985	120.98(3)	2535(150)	3.7266
140.4(1.3)	2.456805	8.033451	6.103889	120.47(4)	2500(100)	3.7197
144.5(1.9)	2.453780	8.001490	6.096827	119.70(4)	2520(160)	3.711

temperature measurement and on the MgO volume determination using X-ray diffraction (the later remaining to about 0.1%). The pressures given by MgO and NaCl standards at room temperature differ by less than 1%. The use of Pt as a pressure standard leads to unreliable results. This could be due to partial reactions or specific physical properties due to the nano-size of Pt particles.

The choice of correct formalisms and approximations is critical to make accurate extrapolations beyond the pressure and temperature conditions of the experiment.

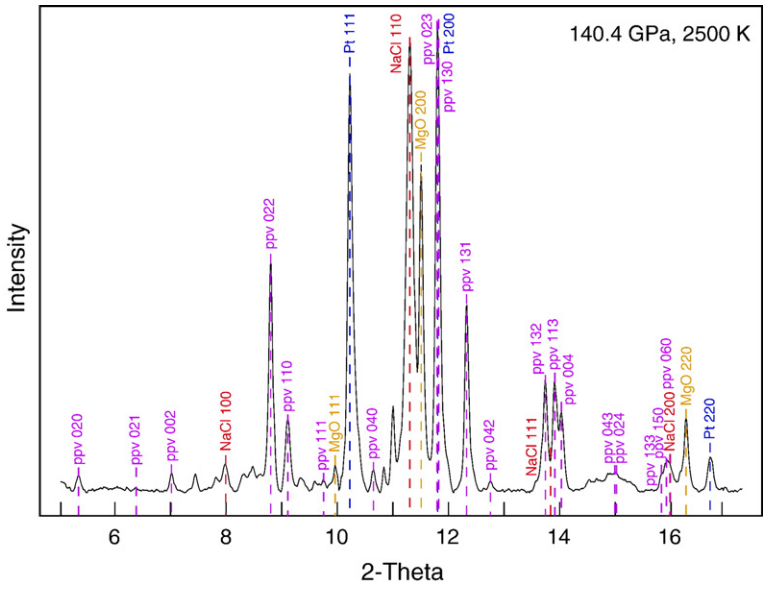

Fig. 1. Diffraction pattern obtained at 140.4 GPa and 2500 K. Sharp peaks correspond to post-perovskite phase, MgO, Pt and NaCl.

Room temperature data is fitted to a third order Birch–Murnaghan EoS. We used the Mie–Grüneisen–Debye model to determine thermal pressure. The Grüneisen parameter is considered to be temperature independent and its volume dependence can be accurately described by the formula $\gamma=\gamma_\infty+(\gamma_0-\gamma_\infty)\,(V/V_0)^\beta$ [14]. We also fitted the thermal pressure component with a thermal expansion model. A polynomial thermal expansion model, including the linear case $\alpha=a+bT$, is often used in the literature. This approach is not accurate at high temperatures as it leads to underestimate thermal expansion when extrapolating with a second degree polynomial, and overestimate it in the linear case. We found that the exponential form $\alpha=\alpha_\infty\,\exp(-b/(1+T))$ is much more accurate to model temperature dependence of thermal expansion, especially by introducing a constant value of α for temperatures well above the Debye temperature. Given the high pressures and the limited pressure range investigated in this study, we can consider as good approximations that thermal expansion does not depend on pressure and that $\mathrm{d}K/\mathrm{d}T$ is constant.

4. Results and discussion

We started the experiment by producing an intimate mixture of $MgSiO_3$ perovskite + MgO at 94 GPa, via the decomposition of Mg_2SiO_4. We observed the perovskite/ppv transformation at 111.1 GPa, after 10 min of laser annealing at 2000 K. The ppv has then been clearly identified up to 144.5 GPa and 2520 K. The diffraction pattern displayed on Fig. 1 represents the overall quality of the diffraction peaks obtained during this experiment. More than 15 sharp ppv reflections were used to refine its unit-cell volume, and peaks of all phases can easily be indexed.

The complete dataset of ppv unit-cell volume, comprising 24 data points at ambient temperature, and an equal number at high temperature, is represented in Fig. 2. The corresponding values are summarized in Table 1.

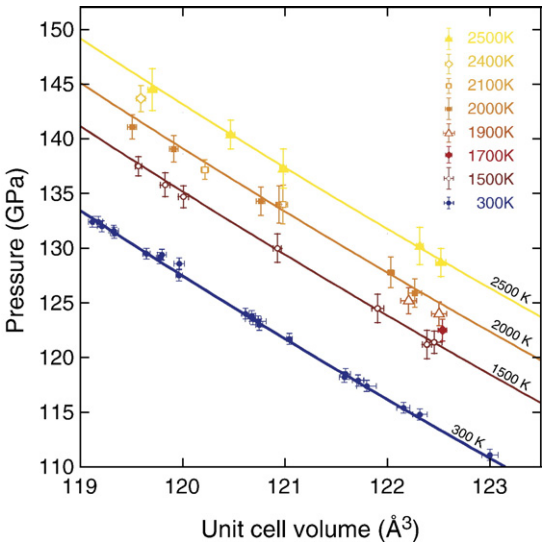

Fig. 2. Collected data points compared to the compression curves calculated by Ono and Oganov [14]. Our results agree very well with the model in the studied P–T range. Note the very good resolution obtained in the present study, the effect of a temperature excess of 100 K on ppv volume being clearly visible above one megabar.

Most of the high temperatures achieved in this experiment are close to 1500 K, 2000 K and 2500 K. All the fitted EoS parameters are summarized in Table 2 together with those of recent studies [14–17]. Note that the room temperature bulk modulus is similar when using NaCl as a pressure standard (232.4(3) GPa instead of 231.2(1) GPa when using MgO). The accuracy of the fits is very good, particularly at high temperature, with Σ (Pcalc − Pobs)^2 = 2.5 to 5 GPa^2, depending on the thermal pressure model used. The agreement with the calculations of Ono and Oganov [14] is excellent in the studied P–T range. A slight shift compared to the Tsushiya et al. [15] model is observed, but their thermal expansion values are found to be very similar to this study. It is thus possible to assert that calculations and experiment converge on the high temperature elastic properties of $MgSiO_3$ ppv phase.

The compression behavior of the ppv phase appears strongly anisotropic. This can be illustrated by the differences in (a, b, c) linear incompressibilities determined using a fitting method described in [18]. We provide here not only 300 K and 0 GPa values, but also those at high pressure and temperature together with thermal expansions on each axis (see Table 3). The compression behavior on each axis is illustrated on Fig. 3. The structure appears to be the less compressible along the c axis with a linear incompressibility close, though significantly higher than the one on a axis. The structure is with no doubt much more compressible along the b axis: 3.7 times more compressible than the c axis at 0 GPa and 300 K, 1.7 time at 136 GPa and 3000 K. These results are in very good agreement with previous calculations [3]. Such an anisotropy previously

Table 2
$MgSiO_3$ ppv P–V–T equation of state parameters

300 K elastic parameters				
	This study	Ono et al. [16]	Shieh et al. [17]	Tsuchiya et al. [15]
V_0 (Å^3)	162.2[a]	162.86[a]	164.9(6)	163.8
K_0 (GPa)	231.2(1)	237(1), 226(1), 248(1)	219(5)	215.9
K'_0	4.0[a]	4.0[a]	4[a]	4.41

HT parameters		
	This study	Ono and Oganov [14]
γ_∞	1.114[a]	1.114
γ_0	1.553[a]	1.553
β	13(1)	4.731
	This study (110–150 GPa)	Tsuchiya et al. [15]
α_∞ (10^{-5}·K^{-1})	1.48(10)	1.58 (100 GPa), 1.40 (125 GPa)
b (K)	396(40)	275 (100 GPa), 289 (125 GPa)
dK/dT (GPa·K^{-1})	−0.015[a]	−0.015

[a] Fixed.

Table 3
$MgSiO_3$ ppv single axis elastic properties

300 K and 0 GPa elastic parameters		
Axis	Unit-cell parameter (Å)	Linear incompressibility (GPa)
a	2.68(2)	855(78)
b	9.35(6)	330(27)
c	6.53(2)	1209(72)

HT elastic parameters (110–150 GPa)			
Axis	dK/dT (GPa·K^{-1})	α_∞ (10^{-5}·K^{-1})	b (K)
a	−0.015[a]	1.64(16)	760(70)
b	−0.015[a]	1.71(17)	319(30)
c	−0.015[a]	1.29(13)	488(50)

Linear incompressibilities (GPa) at HP and HT				
Axis	136 GPa, 3000 K		135 GPa, 4000 K	
	This study	Stackhouse et al. [3]	This study	Stackhouse et al. [3]
a	2010(100)	2020.4	1878(95)	1985.1
b	1401(70)	1543.7	1290(65)	1478.9
c	2370(120)	2345.6	2235(110)	2088.2

[a] Fixed.

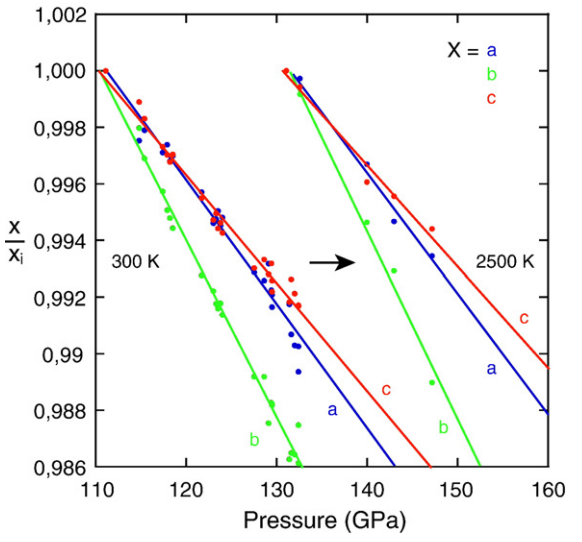

Fig. 3. Evolution of X/X_i with pressure, where X denotes either a, b or c ppv unit-cell parameter and X_i the values of these parameters at the lowest pressures for a given temperature. The ppv structure clearly appears much more compressible along the b axis, and less compressible along the c axis.

pointed out on $MgGeO_3$ analog [19] is to be linked to the $MgSiO_3$ ppv layered structure composed of flat sheets of SiO_6 octahedra placed perpendicularly to the *b* axis [1]. It is less straightforward to understand, however, why the ppv phase is less compressible along the *c* axis where octahedra share corners compared to the *a* axis where octahedra share edges. It is possibly due to the fact that the shortest O–O bonds lie along the c axis. Overall, the elastic anisotropy of the ppv phase appears largely different from that of the perovskite for which the linear compressibilities differ only by about 53% at 0 GPa and 300 K [20]. Therefore, the seismic properties of the deep lower mantle may be considerably affected by any preferential orientation of the ppv phase. However, this preferential orientation is not likely to occur along {010}, but along {110}or {100} instead according to first-principles metadynamics calculations and plastic deformation of $MgGeO_3$ [21,22].

Elastic anisotropy is not the only difference between ppv and perovskite structures. The volume reduction along the phase transition is found to be 1.93% at 130 GPa and 300 K, if compared to perovskite data recently remeasured by Andrault et al. [20]. The experimental *PVT*-EoS available today for the $MgSiO_3$ perovskite may not be of similar accuracy as that of the present study, especially above 100 GPa. Nevertheless, because the ab-initio calculations show similar elastic properties for both $MgSiO_3$ perovskite and ppv phase at pressure and temperature conditions close to that of the phase transitions [15], we can expect a density jump of about 2%. Note that the elasticity of the lower mantle ppv phase may be more complex, since the effects of Al and Fe must be taken into account before drawing any conclusions on the D″ transition. Just like in the pv structure, Al could be present in different sites (octahedral or as a cation in-between the ppv sheets) and Fe could be found with different valences depending on the Fe–Al coupling in the crystal. Present literature is contradictory on that subject, be it from theoretical [23–25], or experimental studies [26–28].

Beyond implications for the deep Earth, we could observe with that study an excellent agreement with calculations. This opens new perspectives of collaborations in the next future.

Acknowledgements

We would like to thank R. Boehler for his work and useful suggestions that helped to improve the laser-heating setup on ID27 beamline of the ESRF and W. A. Crichton for his help on the manuscript.

References

[1] M. Murakami, K. Hirose, K. Kawamura, N. Sata, Y. Ohishi, Post-perovskite phase transition in $MgSiO_3$, Science 304 (2004) 855–858.
[2] A.R. Oganov, S. Ono, Theoretical and experimental evidence for a post-perovskite phase of $MgSiO_3$ in Earth's D″ layer, Nature 430 (2004) 445–448.
[3] S. Stackhouse, J.P. Brodholt, J. Wookey, J.-M. Kendall, G.D. Price, The effect of temperature on the seismic anisotropy of the perovskite and post-perovskite polymorphs of $MgSiO_3$, Earth Planet. Sci. Lett. 230 (2005) 1–10.
[4] E. Schultz, M. Mezouar, W.A. Crichton, S. Bauchau, G. Blattmann, D. Andrault, G. Fiquet, R. Boehler, N. Rambert, B. Sitaud, P. Loubeyre, Double-sided laser heating system for *in situ* high pressure–high temperature monochromatic X-ray diffraction at the ESRF, High Press. Res. 25 (2005) 71–83.
[5] M. Mezouar, W.A. Crichton, S. Bauchau, F. Thurel, H. Witsch, F. Torrecillas, G. Blattmann, P. Marion, Y. Dabin, J. Chavanne, O. Hignette, C. Morawe, C. Borel, Development of a new state-of-the-art beamline optimized for monochromatic single-crystal and powder X-ray diffraction under extreme conditions at the ESRF, J. Synchrotron Radiat. 12 (2005) 659–664.
[6] L.R. Benedetti, P. Loubeyre, Temperature gradients, wavelength-dependent emissivity, and accuracy of high and very-high temperatures measured in the laser-heated diamond cell, High Press. Res. 24 (2004) 423–445.
[7] S.H. Shim, T.S. Duffy, G. Shen, The stability and *P–V–T* equation of state of $CaSiO_3$ perovskite in the Earth's lower mantle, J. Geophys. Res. 105 (2000) 25955–25968.
[8] A.C. Larson, R.B. Von Dreel, GSAS manual, Los Alamos National Laboratory, 1988.
[9] C.S. Zha, H.K. Mao, R.J. Hemley, Elasticity of MgO and a primary pressure scale to 55 GPa, Proc. Natl. Acad. Sci. U. S. A. 97 (2000) 13494–13499.
[10] S. Speziale, C.S. Zha, T.S. Duffy, R.J. Hemley, H.K. Mao, Quasi-hydrostatic compression of magnesium oxyde to 52 GPa: implications for the pressure–volume–temperature equation of state, J. Geophys. Res. 106 (2001) 515–528.
[11] I. Inbar, R.E. Cohen, High-pressure effects on thermal-properties of MgO, Geophys. Res. Lett. 22 (1995) 1533–1536.
[12] B.B. Karki, R.M. Wentzcovitch, S. De Gironcoli, S. Baroni, High-pressure lattice dynamics and thermoelasticity of MgO, Phys. Rev. B61 (2000) 8793–8800.
[13] A.R. Oganov, P.I. Dorogokupets, All-electron and pseudopotential study of MgO: equation of state, anharmonicity, and stability, Phys. Rev. B67 (2003) 224110.
[14] S. Ono, A.R. Oganov, In situ observations of phase transition between perovskite and $CaIrO_3$-type phase in $MgSiO_3$ and pyrolitic mantle composition, Earth Planet. Sci. Lett. 236 (2005) 914–932.
[15] J. Tsushiya, T. Tsushiya, R.M. Wentzcovitch, Vibrational and thermodynamic properties of $MgSiO_3$ postperovskite, J. Geophys. Res. 110 (2005) B02204.
[16] S. Ono, T. Kikegawa, Y. Ohishi, Equation of state of CaIrO3-type MgSiO3 up to 144 GPa, Am. Mineral. 91 (2006) 475–478.
[17] S.R. Shieh, T.S. Duffy, A. Kubo, G. Shen, V.B. Prakapenka, N. Sata, K. Hirose, Y. Ohishi, Equation of state of the postperovskite phase synthesized from a natural $(Mg,Fe)SiO_3$ orthopyroxene, Proc. Natl. Acad. Sci. U. S. A. 103 (2006) 3039–3043.
[18] R.J. Angel, EOS-FIT V5.2 manual, Crystallography Laboratory, 2001.

[19] K. Hirose, K. Kawamura, Y. Ohishi, S. Tateno, N. Sata, Stability and equation of state of $MgGeO_3$ post-perovskite phase, Am. Mineral. 90 (2005) 262–265.
[20] Andrault, D., Bolfan-Casanova, N., Bouhifd, A., Guignot, N., Kawamoto, T., submitted for publication. On the complex role of Al on Al-bearing $(Mg,Fe)SiO_3$ perovskite equation of state at high P and T. Submitted to Earth Planet. Sci. Lett.
[21] A.R. Oganov, R. Martonak, A. Laio, P. Raiteri, M. Parrinello, Anisotropy of Earth's D″ layer and stacking faults in the $MgSiO_3$ post-perovskite phase, Nature 438 (2005) 1142–1144.
[22] S. Merkel, A. Kubo, L. Miyagi, S. Speziale, T.S. Duffy, H.K. Mao, H.-R. Wenk, Plastic deformation of $MgGeO_3$ post-perovskite at lower mantle pressures, Science 311 (2006) 644–646.
[23] R. Caracas, R.E. Cohen, Effect of chemistry on the stability and elasticity of the perovskite and post-perovskite phases in the $MgSiO_3$–$FeSiO_3$–Al_2O_3 system and implications for the lowermost mantle, Geophys. Res. Lett. 32 (2005) L16310.
[24] S. Stackhouse, J.P. Brodholt, G.D. Price, Elastic anisotropy of $FeSiO_3$ end-members of the perovskite and post-perovskite phases, Geophys. Res. Lett. 33 (2006) L01304.
[25] S. Akber-Knutson, G. Steinle-Neumann, P.D. Asimow, Effect of Al on the sharpness of the $MgSiO_3$ perovskite to post-perovskite phase transition, Geophys. Res. Lett. 32 (2005) L14303.
[26] S. Tateno, K. Hirose, N. Sata, Y. Ohishi, Phase relations in $Mg_3Al_2Si_3O_{12}$ to 180 GPa: effect of Al on post-perovskite phase transition, Geophys. Res. Lett. 32 (2005) L15306.
[27] K. Hirose, R. Sinmyo, N. Sata, Y. Ohishi, Determination of post-perovskite phase transition boundary in $MgSiO_3$ using Au and MgO pressure standards, Geophys. Res. Lett. 33 (2006) L01310.
[28] R. Sinmyo, K. Hirose, H.S. O'Neill, E. Okunishi, Ferric iron in Al-bearing post-perovskite, Geophys. Res. Lett. 33 (2006) L12S13.